Supporting Information

The Spatial Resolution Limit for Individual Domain Wall in Magnetic Nanowires

Sumit Dutta,[†,#] *Saima A. Siddiqui,*[†,#] *Jean Anne Currivan-Incorvia,*[‡] *Caroline A. Ross,*[§,*] *and Marc A. Baldo*[†,*]

† Department of Electrical Engineering and Computer Science, Massachusetts Institute of Technology, Cambridge, MA 02139, USA

‡ Department of Physics, Harvard University, Cambridge, MA 02138, USA

§ Department of Materials Science and Engineering, Massachusetts Institute of Technology, Cambridge, MA 02139, USA

# These authors contributed equally to this work.

* To whom correspondence should be addressed. Email addresses: (M. A. Baldo) baldo@mit.edu ; (C. A. Ross) caross@mit.edu

Nanowire Fabrication. We fabricated 80-nm-wide Co wires as shown in Figure 1a-b. The fabrication process started with the deposition of thin films composed of nominally Ta(5 nm)/Co(8 nm)/Au(3 nm) using ion-beam sputtering at a base pressure of 5×10^{-8} torr, Ar pressure of 1×10^{-4} torr and target power of 920 W over 3" diameter targets yielding deposition rates of 0.029 nm s^{-1}. The saturation magnetization of the film suggested an actual Co thickness of 5 nm. The films were patterned into rings using a poly (methyl methacrylate) (PMMA)/hydrogen silsesquioxane (HSQ) bilayer resists and ion beam etching.[1] First, we spun 2% PMMA and then 2% HSQ on the thin film. Then the HSQ was exposed with an Elionix ELS-F125 electron beam lithography tool operated at 125 keV and 19.2 mC cm^{-2} dose. The exposed HSQ was developed with salty developer (1 wt % NaOH and 4 wt % NaCl in deionized water) at room temperature and the underlying PMMA was later removed with oxygen plasma except under the HSQ patterns. Using the bilayer resist as an etch mask, the metal film was ion-beam etched with Ar^+ at 0.45 kV accelerating voltage and the resist stack was removed with N-methyl-2-pyrrolidone heated at 135°C on a hot plate. Further details of the patterning process are found in reference (1). The root-mean-square (RMS) edge roughness of fabricated Co wires is ~2 nm.

Domain Wall Traveling Distance Measurements. Our experiment was designed to understand how domain wall pinning sites are distributed in sub-100-nm-wide magnetic wires. We measured the edge deviations in our wires using scanning electron micrographs and measured domain wall positions using magnetic force micrographs.[2] The concentric rings in Figure 5 had domain walls initialized with a 239 kA/m magnetic field to saturate the rings in the $+x$ direction, resulting in remanent onion states with two 180° domain walls (one head-to-head, one tail-to-tail) along the diameter in each ring.[3,4] Figure S1 shows a magnetic force micrograph of domain walls initialized with a 239 kA/m magnetic field to saturate the rings in the $+x$ direction, resulting in

remanent onion states. Circular rings and the curvature in L-shaped nanowires with similar radii (5–5.5 μm) were used for convenience in nucleating domain walls with an applied field; the walls then relaxed toward nearby pinning sites at remanence. After nucleating the tail-to-tail domain walls, we applied the magnetic field along the length of the wires to move them and imaged their final positions afterwards. When the applied field was high enough to depin the domain walls, they started moving and were eventually trapped by the next pinning site that was sufficient to prevent further motion. Domain walls were re-nucleated for each applied magnetic field value, and we recorded both their initial and final positions. The traveling distances below 2.5 μm were taken from the concentric rings and those above 2.5 μm were taken from the L-shaped nanowires. In the concentric rings the field component along the wire falls by only <10% after 2.5 μm domain wall motion due to curvature of the wire. Figure S2 shows magnetic force micrographs of the L-shaped nanowires for the different applied fields.

The domain walls in the nanowires experienced the magnetic stray field from the magnetic force microscope probes during scanning which can perturb their positions. To exclude this possibility, we note there was no dragging of domain walls evident in low-resolution (large scan area) magnetic force micrographs. The dragging effect is more prominent in samples imaged after applying small fields and it decreases with higher applied fields. Domain wall displacements showing any evidence of domain wall dragging by the probe were removed from the statistical analysis. Otherwise, magnetic force microscopy is considered as a noninvasive process, and domain wall positions can be determined to within 50 nm.

The translation of domain walls in the nanowire rings required fields > 16 kA/m, much higher than the coercive field of the continuous Co film, which is 2 kA/m. Figure 5 shows the magnetic force micrographs of nanowire rings after applying different magnetic fields along the

wire. The average traveling distances of the domain walls increased with field, but some of the domain walls remained at the same position even after applying a higher magnetic field. For example, the domain wall marked by a black arrow in Figure 5 remained at the same position at 20 kA/m and 24 kA/m, was translated after applying 28 kA/m, then remained pinned at 32 kA/m. Similarly, the domain wall marked by the white arrow changed its position when the field increased from 20 kA/m to 24 kA/m and remained at that site at 28 kA/m and 32 kA/m. In this case, the depinning field of the first site was between 20 kA/m and 24 kA/m, and the second was more than 32 kA/m.

Interactions between domain walls in adjacent nanowires are neglected in this analysis. Based on the wire geometry and domain wall structure, we calculate from micromagnetics that the maximum field that one domain wall exerts on its neighbor is ~16 kA/m. This is smaller than the fields applied to depin the walls. The effects of interactions were investigated using a sample with more closely spaced wires, which led to correlated motion of domain walls. These results will be discussed elsewhere.

Micromagnetic Modeling. We modeled IMA Co wires with a micromagnetic solver, the Object-Oriented Micro-Magnetic Framework (OOMMF), which provides a deterministic solution to the Landau-Lifshitz-Gilbert (LLG) equation.[5] The Co wires were modeled using: damping parameter $\alpha = 0.018$, saturation magnetization $M_{sat} = 1.40 \times 10^6$ A/m, a uniaxial magnetocrystalline anisotropy of 4100 J/m^3 with random direction in each cell, a wire thickness of 5 nm, and a cell size of 3 nm × 3 nm × 2.5 nm. In our modeled PMA CoFeB wires, we used: $\alpha = 0.01$, $M_{sat} = 7.96 \times 10^5$ A/m, an anisotropy in the out-of-plane direction of $K_z = 7.82 \times 10^5$ J/m^3 with an additional random-direction anisotropy in each cell of 100 J/m^3, a wire thickness of 5 nm, and a cell size of

3 nm × 3 nm × 2.5 nm. For IMA and PMA, the exchange constant = 10^{-11} J/m. These parameters are justified in our previous study.[6]

The cell size (3 nm) is smaller than the grain size of the Co (estimated as 5-10 nm) therefore in the model the magnetocrystalline anisotropy fluctuates on a smaller length scale than expected in the physical system. However, both lengthscales are much smaller than the domain wall width or the edge roughness correlation length and the effects of the small cell size are not believed to significantly affect the analysis.

In our micromagnetic modeling of synthetic wires, we chose a wire length of 1.26 μm because that is significantly longer than ξ = 255 nm. This wire length supported a distribution of pinning sites while minimizing the computation time needed, which grows by the cube of wire length. We fixed the magnetization direction in the left and right ends of the wire to ensure a domain wall is nucleated in the wire. To limit the perturbation of the domain wall by the fringing field from these fixed ends, the simulated wire included a smooth region 150 nm long on the left and right of the 1.26-μm-long region with line edge roughness. About 40% of the domain walls in simulated wires did not move due to the stray field. These were discarded from the data. The discretization of wire edges into cells for micromagnetic modeling results in pinning fields whose scale may not agree with pinning fields in experimental measurements, but the models still agree qualitatively with experiments.[7] The wire size chosen was long enough for a full range of motion while allowing for a large sample size.

The domain walls have a transverse structure with the magnetization of the core along *y*, transverse to the wire. Although a domain wall may be affected by one wire edge more than the other based on its core magnetization direction,[8,9] our simulation data and analytical models used

a large number of non-deterministic edge profiles and thus were not biased by the fact that we set domain wall core magnetization in the $+y$ direction.

Figure S3 shows a domain wall in an IMA wire and a PMA wire in micromagnetic models. The typical domain wall widths in IMA wires and PMA wires are ~40 nm and ~10 nm, respectively.

Power Spectral Density (PSD) Calculations. The PSD of synthesized self-affine and random-edge profiles in Figure 1d is the average PSD of 10^4 such synthesized edges in order to reduce the variation of points typically seen in the PSD of only one wire edge. This shows the characteristic PSD of self-affine and random-edge profiles without wire-to-wire variations. A standard rectangular window is used for the PSD of the self-affine and random-edge profiles. However, for the PSD of the single discretized wire edge, the Hann window is used because it has low aliasing, which is useful considering the fewer number of points especially at low spatial frequency in the single discretized wire edge. The discretized wire edge is taken from a scanning electron micrograph of 1024×1024 pixels with a 1 nm pixel size. All wire edges in Figure 1d have a root-mean-square line edge roughness of 3 nm.

Domain Wall Position Spacing Models. The Δx distributions in Figure 3 are from extensive micromagnetic modeling of individual wires. For each wire, there is a simulation for each of the 421 3-nm-long cells in which a domain wall could be initialized. Hence, the number of wires for each histogram in Figure 3 is much smaller than the number of wires simulated for each applied H field in Figure 4.

Analytical Models: The analytical model $(-df/dx)_{mean}$ is found by solving Equation (2) with Equation (1) by separating variables:

$$f(x) = \exp\left(-\frac{x}{l_0}\right)\prod_{p=1}^{\infty}\exp\left(\frac{kB_{LER}C_p\xi}{2\pi}\frac{\nu^{-p(H_Q+1)}}{\cos\Psi_p}\left(\cos\Phi_p - \cos\left(\frac{2\pi}{\xi}\nu^p\left((x-x_{min})\cos\Psi_p\right)+\Phi_p\right)\right)\right) \tag{S1}$$

$$-\frac{df}{dx} = -\left(-\frac{1}{l_0} + kB_{LER}\sum_{p=1}^{\infty}C_p\nu^{-pH_Q}\sin\left(\frac{2\pi}{\xi}\nu^p\left((x-x_{min})\cos\Psi_p\right)+\Phi_p\right)\right)$$
$$\times\exp\left(-\frac{x}{l_0}\right)\prod_{p=1}^{\infty}\exp\left(\frac{kB_{LER}C_p\xi}{2\pi}\frac{\nu^{-p(H_Q+1)}}{\cos\Psi_p}\left(\cos\Phi_p - \cos\left(\frac{2\pi}{\xi}\nu^p\left((x-x_{min})\cos\Psi_p\right)+\Phi_p\right)\right)\right) \tag{S2}$$

$$\left(-\frac{df}{dx}\right)_{mean} = \frac{1}{N}\sum_{w=1}^{N}\left(-\frac{df}{dx}\right)_w \tag{S3}$$

We use $-df/dx$ because it is the derivative of $1 - f$ that gives how many DWs are trapped at a certain distance x. We expect $df/dx < 0$ because $f(x = 0) = 1$ and f decreases with x until all domain walls have been trapped. We determine the analytical model $(-df/dx)_{mean}$ in Equation (S3) by calculating Equation (S2) for $N = 1500$ wires. The coefficient k, which weights the edge profile $\Delta y(x)$ in the substitution of Equation (1) in Equation (2), represents the magnitude of width effects and is chosen such that $(-df/dx)_{mean}$ is still positive and the total area under the curve converges to unity.

The simplified analytical model given in Equation (3) is solved as follows:

$$-\frac{df}{dx} = -\left(-\frac{1}{l_0} + b\exp(-x/\lambda)\right)\exp\left(-\frac{x}{l_0} + b\lambda\left(1-\exp(-x/\lambda)\right)\right) \tag{S4}$$

References:

(1) Currivan, J. A.; Siddiqui, S. A.; Ahn, S.; Tryputen, L.; Beach, G. S. D.; Baldo, M. A.; Ross, C. A. *J. Vac. Sci. Technol. B*, **2014**, *32*, 021601.

(2) Huang, X. P.; Shi, Z. L.; Wang, M.; Konoto, M.; Zhou, H. S.; Ma, G. B.; Wu, D.; Peng, R.; Ming, N. B. *Adv. Mater.*, **2010**, *22*, 2711.

(3) Rothman, J.; Kläui, M.; Lopez-Diaz, L.; Vaz, C. A. F.; Bleloch, A.; Bland, J. A. C.; Cui, Z.; Speaks, R. *Phys. Rev. Lett.*, **2001**, *86*, 1098-1101.

(4) Li, S. P.; Peyrade, D.; Natali, M.; Lebib, A.; Chen, Y.; Ebels, U.; Buda, L. D.; Ounadjela, K. *Phys. Rev. Lett.*, **2001**, *86*, 1102-1105.

(5) OOMMF: Object Oriented MicroMagnetic Framework **2002**, http://math.nist.gov/oommf.

(6) Dutta, S.; Siddiqui, S. A.; Currivan-Incorvia, J. A.; Ross, C. A.; Baldo, M. A. *AIP Adv.*, **2015**, *5*, 127206.

(7) Jiang, X.; Thomas, L.; Moriya, R.; Parkin, S. S. P. *Nano Lett.*, **2011**, *11*, 96-100.

(8) Hayashi, M.; Thomas, L.; Rettner, C.; Moriya, R.; Parkin, S. S. P. *Nat. Phys.*, **2007**, *3*, 21-25.

(9) Jang, Y.; Bowden, S. R.; Mascaro, M.; Unguris, J.; Ross, C. A. *Appl. Phys. Lett.*, **2012**, *100*, 062407.

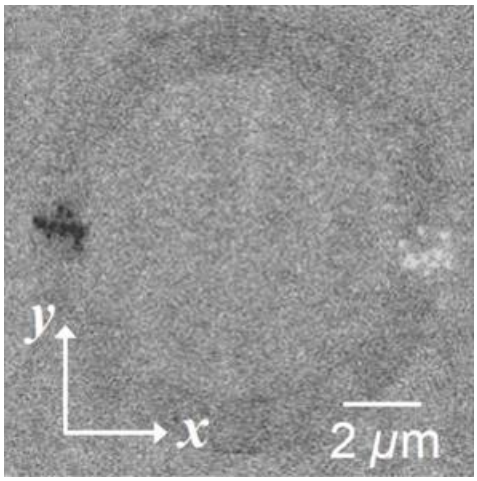

Figure S1. Magnetic force micrograph of domain walls in the initial onion states.

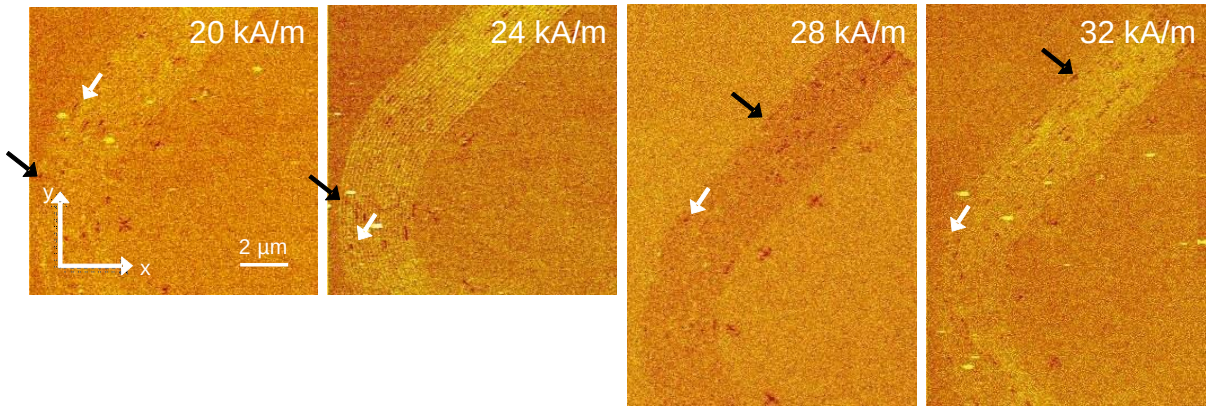

Figure S2. Magnetic force micrographs of L-shaped nanowires.

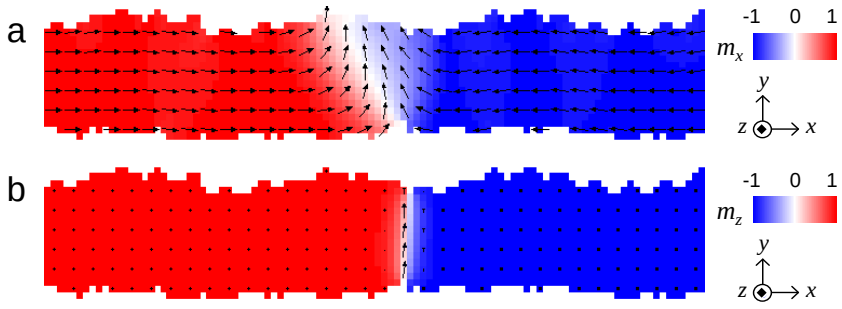

Figure S3. A single domain wall as seen in a close-up top-down view of the magnetic moments, m_x and m_z, in micromagnetic models of (a) an IMA wire and (b) a PMA wire, respectively.